AIP Journal of Applied Physics

Theoretical examination of superconductivity in the cubic antiperovskite Cr3GaN under pressure

H. M. Tütüncü and G. P. Srivastava

Citation: Journal of Applied Physics **114**, 053905 (2013); doi: 10.1063/1.4817072
View online: http://dx.doi.org/10.1063/1.4817072
View Table of Contents: http://scitation.aip.org/content/aip/journal/jap/114/5?ver=pdfcov
Published by the AIP Publishing

JOURNAL OF APPLIED PHYSICS **114**, 053905 (2013)

Theoretical examination of superconductivity in the cubic antiperovskite Cr_3GaN under pressure

H. M. Tütüncü[1] and G. P. Srivastava[2]
[1]*Fen-Edebiyat Fakültesi, Sakarya Üniversitesi, Fizik Bölümü, 54187 Adapazar i, Turkey*
[2]*School of Physics, University of Exeter, Stocker Road, Exeter EX4 4QL, United Kingdom*

(Received 18 April 2013; accepted 15 July 2013; published online 5 August 2013)

We present results of a first-principles investigation of the lattice dynamics and electron-phonon coupling of Cr_3GaN under pressure within a linear response approach based on density functional perturbation theory. It is found that stable phonon modes are maintained throughout the Brillouin zone in the pressure range 0-100 GPa. Our results at zero pressure indicate that the material is a conventional electron-phonon superconductor with intermediate level of coupling strength. It is further found that the decrease in the density of states at the Fermi level and the increase of phonon frequencies under pressure are the main causes for a monotonic decrease of the electron-phonon coupling parameter and the superconductor transition temperature. © *2013 AIP Publishing LLC*. [http://dx.doi.org/10.1063/1.4817072]

I. INTRODUCTION

In recent years, the cubic antiperovskite materials have received great attention since the discovery of 8 K superconductivity in $MgCNi_3$.[1,2] This transition is unexpected due to the large Ni content in this material, which may favor a magnetic ground state rather than superconducting state. This raises a question on the effects of magnetism on the superconducting properties of this material. In the experimental work of Rosner *et al.*,[3] it was suggested that magnetic interactions can support superconductivity in this cubic antiperovskite. Later studies found that this material shows an s-wave BCS superconductivity,[4–7] and its physical, chemical, and superconducting properties can clearly be understood by considering its electronic structure. This led to several experimental and theoretical efforts to investigate the electronic properties of this cubic antiperovskite. Experimental investigations include photoemission and x-ray absorption measurements.[8] On the theoretical side, it includes the self-consistent tight-binding linear muffin-tin orbital (TB LMTO),[9] the linear muffin tin orbital (LMTO) method,[4,10] the full-potential augmented plane wave (FLAPW) method,[11,12] and density-functional theory within the local-density approximation.[11,13–15] These experimental and theoretical studies showed that the significant feature of the electronic structure of $MgCNi_3$ is an extended van Hove singularity which creates a large density of states (DOS) just below the Fermi level. In order to achieve a better understanding of superconductivity, phonon properties of this material have been studied experimentally as well as theoretically. Time-dependent inelastic neutron-scattering measurements[16] have been used to obtain the generalized phonon density of states. Phonon dispersion curves for this material have been measured by using inelastic x-ray scattering method.[17] Dynamical properties of $MgCNi_3$ have also been studied by employing different levels of theoretical approaches.[15,16,18,19]

Among $MgCNi_3$'s isostructural cubic antiperovskites $ACNi_3$ (A = Cd, Zn, Al, and Ga), only $CdCNi_3$ demonstrates superconductivity.[20] This has led to studies of the electronic properties of $CdCNi_3$. Theoretical works indicate that this compound, like $MgCNi_3$, is almost ferro-magnetic due to the existence of a large peak in the density of states slightly below the Fermi level, which is favourable to superconductivity. Further theoretical work on phonon spectrum, phonon linewidths, and electron-phonon coupling parameter[21] has confirmed the experimental work that $CdCNi_3$ is a BCS-type superconductor with electron-phonon interaction of medium strength.

Recently, the discovery of a new superconducting ($T_C \sim 3$ K) cubic antiperovskite $ZnNNi_3$ has been reported in the experimental work of Uehara *et al.*[22,23] This material is the third Ni-rich antiperovskite series and the first antiperovskite nitride superconducting material. The discovery of superconductivity in $ZnNNi_3$ has motivated several groups[24–29] to study the structural and electronic properties of this material. Very recently, attention has been directed to Cr-rich intermetallic antiperovskite materials because many of Cr compounds show superconductivity.[30–33] The band structures for Cr_3GaN and Cr_3RN intermetallic antiperovskites have been investigated using the Korringa-Kohn-Rostoker method.[34] This theoretical study pointed out the possibility of superconductivity onset in these compounds due to the calculated high values of McMillan-Hopfield parameter (electronic part of electron-phonon coupling constant). However, this work[34] did not consider the phonon part of electron-phonon coupling constant. Realising the importance of the phonon influence on the superconducting properties of this material, we have recently performed a first-principles theoretical investigation of the structural, electronic, vibrational, and superconducting properties of the cubic antiperovskite Cr_3RhN.[35] This study illustrated that Cr_3RhN is dynamically stable, as no instabilities in the phonon dispersion curves have been found. The calculated superconducting transition temperature T_C value of around 17 K for Cr_3RhN (Ref. 35) is much higher than the corresponding value of 8 K for $MgCNi_3$.

Motivated by our results for Cr_3RhN,[35] in this work, we present a study the structural and electronic properties of

Cr-rich nitride cubic antiperovskite Cr_3GaN using the *ab initio* pseudopotential method based on a generalized gradient approximation (GGA) of the density functional theory. Differences in the electronic structure and electronic density of states between Cr_3GaN and its isostructural compound Cr_3RhN (Ref. 35) are investigated and discussed. We have further carried out *ab initio* linear response calculations of the lattice dynamics, electron-phonon interaction, and polarization characteristics of zone-centre phonon modes. The structural stability of Cr_3GaN has been studied under high pressure (from 0 GPa to 100 GPa). We have also presented the variations of the electron-phonon coupling parameter and T_C with increasing pressure. Finally, differences in the Eliashberg function $\alpha^2F(\omega)$ and superconducting parameters between Cr_3GaN and its isostructural compound Cr_3RhN are investigated and discussed.

II. THEORY

In this work, we have carried out first principle calculations based on the density functional theory, as implemented in the QUANTUM ESPRESSO code.[36,37] The electronic exchange-correlation energy interaction has been treated within the GGA, using the Perdew-Burke-Ernzerhof (PBE) functional theory.[38] The electron-ion interaction was described by using ultrasoft pseudopotentials.[39,40] The wave function was expanded in plane waves with the energy cutoff of 60 Ry, and the electronic charge density was expanded with the energy cut off up of 240 Ry. The Kohn-Sham equations were solved using an iterative conjugate gradient scheme to obtain energy. Brillouin zone integration were performed using the $24 \times 24 \times 24$ Monkhorst-Pack **k**-point mesh.[41]

Phonon spectrum and density of states for Cr_3GaN were obtained in the framework of the harmonic approximation to the force constants and using the linear response method[36,37] which is realized in the QUANTUM ESPRESSO code.[36,37] Within this scheme, second order derivatives of the total energy were calculated to obtain the dynamical matrix. A static linear response of the valence electrons was considered in terms of the variation of the external potential corresponding to periodic displacements of the atoms in the unit cell. The screening of the electronic system in response to the displacement of the atoms was taken into account in a self consistent manner. Integration up to the Fermi surface is done with the smearing technique with the smearing parameter $\sigma = 0.02$ Ry. For phonon calculations, we have used a $12 \times 12 \times 12$ **k** mesh for the Brillouin zone integration. Dynamical matrices have been computed on a $4 \times 4 \times 4$ **q** point mesh, and a Fourier interpolation has been used to calculate phonons for any chosen **q** point.

For calculating the superconducting properties, the Migdal-Eliashberg approach[42,43] has been implemented using the linear response method.[15,44–46] The matrix element for electron-phonon interaction and the Eliashberg function have been evaluated numerically, as described in our previous papers (see, e.g., Ref. 46). The superconductor transition temperature (T_C) was computed by using the McMillan modification of the Allen-Dynes formulation.[47–49]

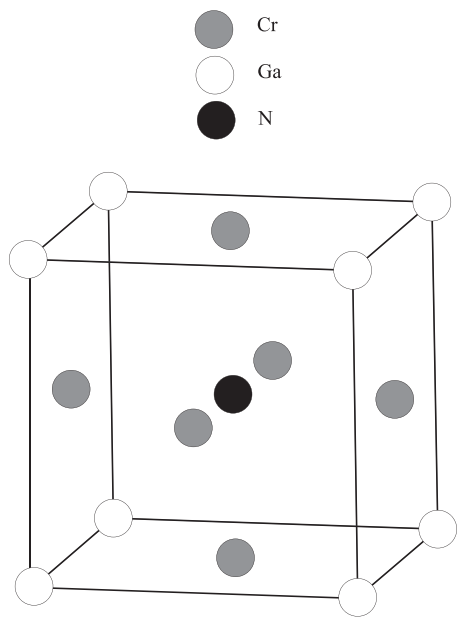

FIG. 1. The cubic antiperovskite structure of Cr_3GaN.

III. RESULTS

A. Structural and electronic properties

Cr_3GaN crystallizes in the cubic antiperovskite structure with the space group $Pm\bar{3}m$. In this structure, as shown in Fig. 1, six Cr atoms occupy the face-centered positions of unit cell forming a three-dimensional network of Cr_6 octahedron, N atoms occupy the body-centered cubic position surrounded by the Cr_6 octahedron cage, and Ga atoms are located at the corners of the unit cell. Table I shows our calculated structural parameters, together with available experimental[50] and other theoretical data.[34] One can see that our calculated lattice constant is larger than the local-density approximation (LDA) value of 3.79 Å (Ref. 34) but only 1.4% smaller than the experimental value of 3.88 Å. Unfortunately, there are no experimental and theoretical data for bulk modulus (B) and its pressure derivative (B') for us to compare with. We have also compared the calculated structural results for Cr_3GaN with those for its isostructural superconducting counterpart Cr_3RhN.[35] The substitution of Rh by Ga mainly affects the bulk modulus value rather than the lattice constant value: the bulk modulus for Cr_3GaN differs from that for Cr_3RhN by 11%. The near equality of the lattice constants of these isostructural compounds is expected

TABLE I. The calculated structural parameters for the cubic antiperovskite Cr_3GaN. The obtained results are also compared with those for the cubic antiperovskite Cr_3RhN and available experimental results.

Cubic antiperovskite	a (Å)	B (Mbar)	B′
Cr_3GaN	3.82	2.30	4.46
LDA (Ref. 34)	3.79		
Experimental[50]	3.88		
Cr_3RhN (Ref. 35)	3.81	2.59	4.32
LDA (Ref. 34)	3.71		
Experimental[50]	3.86		

because the atomic radius of Rh and Ga atoms are 1.35 pm and 1.34 pm, respectively.

Before discussing our electronic results, we have to mention that Cr_3GaN is not magnetic because the spin-down and spin-up electronic structures for this material are found to be exactly the same. Fig. 2 shows the electronic band dispersion curves of Cr_3GaN along several high symmetry directions of the simple cubic Brillouin zone, calculated at the equilibrium lattice constant using the GGA-PBE approximation. The overall band profile for Cr_3GaN is found to be in fairly good agreement with previous theoretical calculations.[34] The total, and site decomposed, electronic DOS are displayed in Fig. 3(a). From the band structure, it is seen that the low-lying band has a parabolic shape along all the considered symmetry directions. This band is mainly dominated by N 2 s electrons and lies between −18 and −15 eV. Above this band, there is a considerably flat band with an energy of −14.60 eV, originating from the 3d electrons of Ga atoms. For energy window from −9 to −5 eV, the Cr electronic states (of s, p, and d orbital nature) hybridize with N 2 p and Ga 4 s states. The bands between −5 and −2 eV are mainly build up from Cr 3d states with some contributions from the 4 p orbitals of Ga atoms. The contributions from other electrons to these bands are negligibly small. Cr 3d states contribute significantly to the bands close to the Fermi level.

Because the DOS distribution near the Fermi level (E_F) plays an important role in determining superconducting properties, it is important to examine the DOS in the vicinity of the Fermi level. We have observed a sharp peak at $E_F \sim 0.7$ eV which is created by the 3d electrons of Cr atoms. We have to mention that a sharp peak in the DOS near E_F has also been noted for $MgCNi_3$ and $CdCNi_3$ (Refs. 15 and 21) which are superconductors. In agreement with the superconductor transition metal carbides such as CrC, NbC, and VC,[33,51] the Fermi level for Cr_3GaN lies on a sharply increasing peak at $E_F + 0.47$ eV. This peak is mainly dominated by the 3d orbitals of Cr atoms. A similar peak with an energy of $E_F + 0.34$ eV is found in the electronic density of states for the superconductor CrC.[33] We note, however, that the numerical values of the DOS at the Fermi level ($N(E_F)$) is 5.00 states/eV for Cr_3GaN, which is lower than the corresponding value of 6.16 states/eV for Cr_3RhN obtained in our previous work.[35] The contribution of Cr atoms to $N(E_F)$ accounts for 97% and Ga atoms for 2%, while the contribution of N atoms is rather small, only 1%. Thus, nitrogen and gallium atoms do not contribute significantly to the DOS at the Fermi level and therefore are not involved in the conduction properties of Cr_3GaN. In contrast, the corner Rh atom in Cr_3RhN makes a considerable contribution to $N(E_F)$.[34,35] It is this difference that makes the value of $N(E_F)$ for Cr_3RhN higher than the corresponding value for Cr_3GaN. Obviously, it is the 3d states of Cr atoms that give rise to the electrical conductivity in Cr_3GaN, though d electrons are generally considered as less efficient conductors.

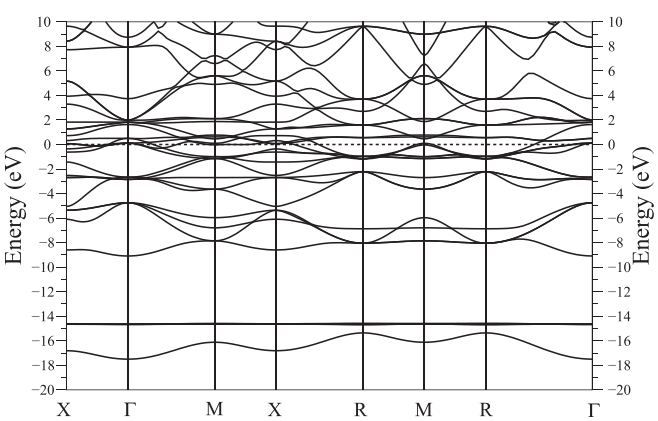

FIG. 2. The electronic structure of Cr_3GaN in the cubic antiperovskite structure. The dashed horizontal line at 0 eV denotes the Fermi level, E_F.

The pressure dependence of the DOS for Cr_3GaN is shown in Fig. 3(b). The effect of pressure is to redistribute the peaks close to the Fermi level: the peaks on either side of the Fermi level are decreased in their height. The weak shoulder at E_F for $P = 0$ becomes sharper as the pressure increases. In order to a better understanding of the pressure effect on the electronic properties of the cubic antiperovskite Cr_3GaN, we have performed the calculation of total DOS at the Fermi level at different pressures. Fig. 4 shows the change of $N(E_F)$ with pressure. As can be seen from this figure, $N(E_F)$ decreases with increase of pressure. In particular, $N(E_F)$ diminishes from 5.00 States/eV to 3.20 States/eV as pressure increases from 0 GPa to 100 GPa. The effect of pressure on the electron-phonon coupling parameter λ is directly related to the change in $N(E_F)$, following the McMillan-Hopfield expression $\lambda = \frac{N(E_F)\langle I^2\rangle}{M\langle\omega^2\rangle}$, where $\langle I^2\rangle$ is the averaged square of the electron-phonon matrix, $\langle\omega^2\rangle$ is the averaged square of the phonon frequency, and M is the mass involved.

B. Phonons and superconductivity

The primitive cell of this material contains five atoms, giving a total of 15 phonon branches including three acoustic branches. The calculated phonon dispersion curves along the high-symmetry lines in the Brillouin zone are shown in Fig. 5(a). The total phonon spectrum has an energy range of about 21 THz. In particular, the phonon dispersions show a set of 12 bands extending up to around 11 THz, separated by a gap of 8.4 THz from three high-frequency bands that lie between 19 and 21 THz. Also, all phonon modes exhibit positive frequencies, strongly suggesting that the optimized Cr_3GaN structure is dynamically stable. The highest three phonon branches are dominated by the motion of nitrogen atoms. These branches are dispersive but the highest of them is nearly flat along the M-X, X-R, and R-M symmetry directions. In the lowest region of the phonon spectrum, we have observed several bands which exhibit dispersive character. This indicates strong interaction between Cr and Ga atoms. The calculated total and partial phonon density of states are presented in Fig. 5(b). The partial DOS shows that the states from 4 THz to 6 THz arise from vibrations of Cr and Ga atoms and the features between 7 and 9 THz are created by the motions of Cr atoms with a very small admixture of N atoms. The sharp peak at 6.2 THz is due to the flatness of T^2_{1u} mode along the $\Gamma - X$ symmetry directions. The sharp peak with the frequency of 10.7 THz also results from the displacements of Cr atoms. From this picture, it can be

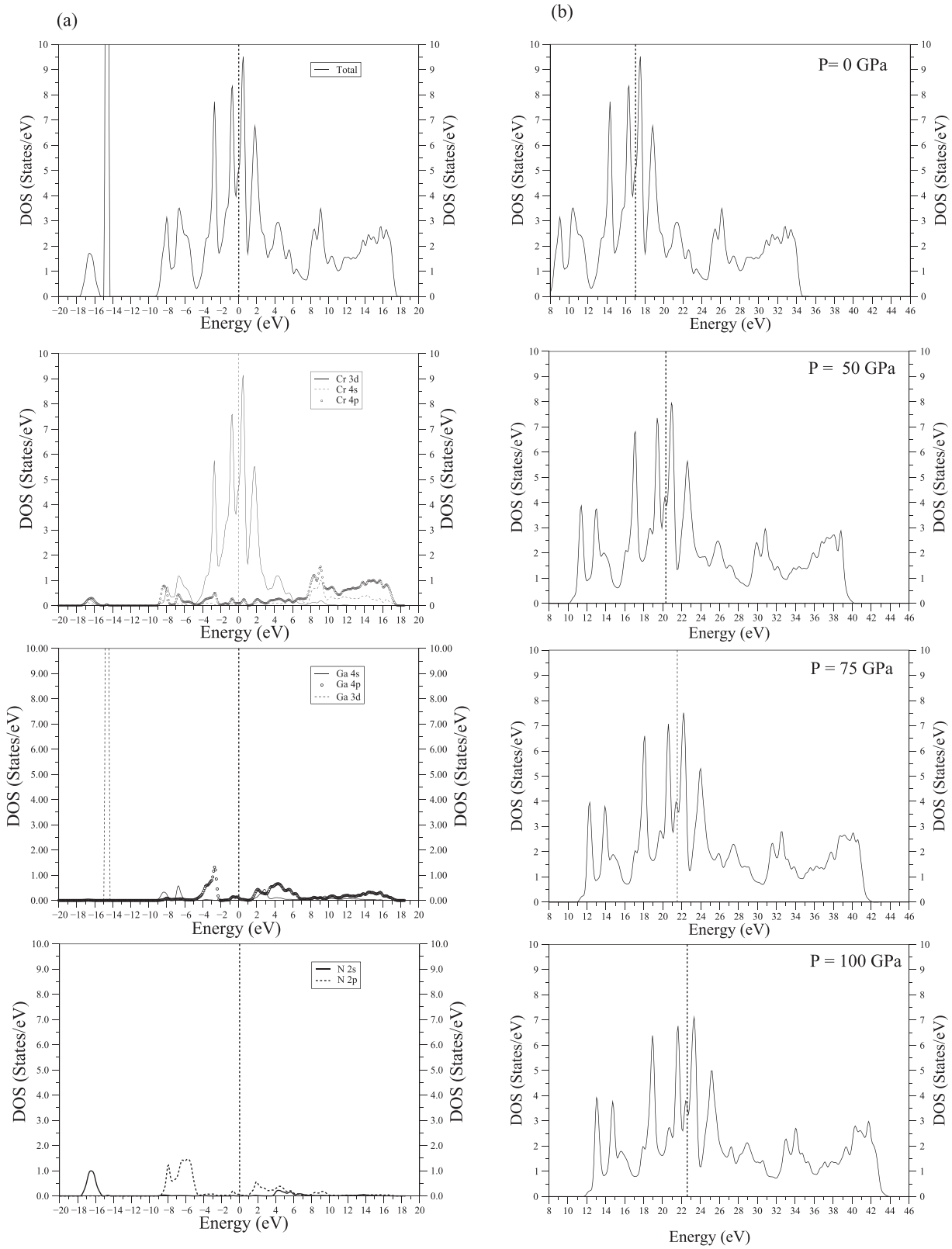

FIG. 3. (a) Total and partial electronic density of states for Cr_3GaN in the cubic antiperovskite structure. The position of the Fermi level is shown by dashed line. (b) Total electronic density of states for the cubic antiperovskite Cr_3GaN at different pressures. The position of the Fermi level is shown by the dashed vertical line.

expected that Cr vibrational modes would make a large contribution to electron-phonon interaction in Cr_3GaN. There is a large gap of 8.4 THz separating the upper sharp peaks at 20.2 and 21.6 THz. Both of these peaks are mainly localized on the N atoms but the lower peak includes a little contribution from Cr vibrations.

At the Γ point of Brillouin zone, the phonon modes in the cubic antiperovskite structure decompose according to

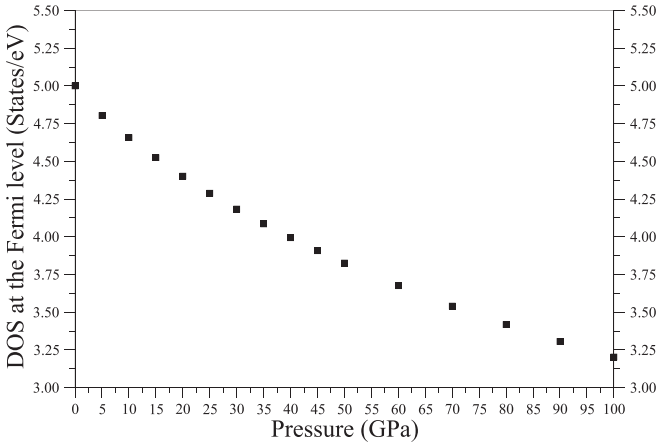

FIG. 4. Predicted pressure dependence of the density of stated at the Fermi level for Cr_3GaN.

the irreducible representation characteristic for the O_h^1 point group

$$\Gamma_{ac} = T_{1u}^{ac} \quad \text{and} \quad \Gamma_{opt} = T_{2u} + T_{1u}^1 + T_{1u}^2 + T_{1u}^3,$$

for acoustic and optical modes, respectively. None of the triply degenerate optical modes is Raman active, as a perfect cubic structure, all lattice sites have inversion symmetry.

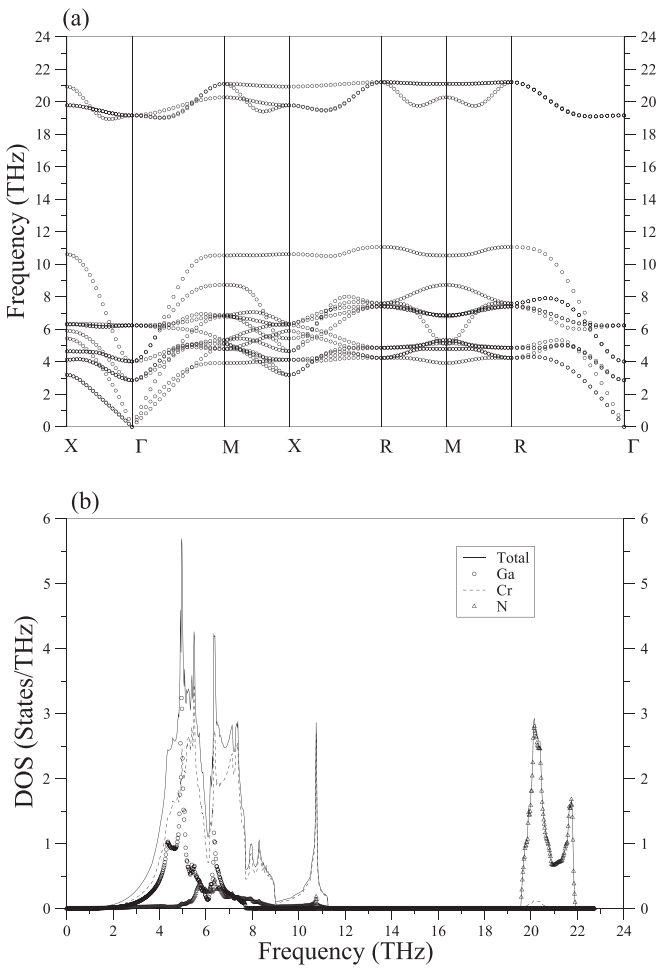

FIG. 5. (a) The calculated phonon dispersion curves along high symmetry directions in Brillouin zone for the cubic antiperovskite Cr_3GaN. (b) Total and partial phonon density of states for Cr_3GaN.

However, these phonon modes can be detected using infrared and neutron spectroscopic techniques. The frequencies of the optical phonon modes are calculated to be 2.86 THz (T_{2u}), 4.02 THz (T_{1u}^1), 6.24 THz (T_{1u}^2), and 19.16 THz (T_{1u}^3). The T_{2u} mode is totally dominated by the vibrations of Cr atoms. The first T_{1u} mode is created by the vibrations of all atoms in the unit cell with the maximum contribution coming from Cr atoms. The intermediate T_{1u} mode results from opposing motions of Ga and Cr atoms. The highest optical phonon mode is due to the vibrations of N atoms with a small contribution from Cr atoms.

Since Cr_3GaN is isostructural to Cr_3RhN and the ionic radii and local bonding environment of these compounds are similar, the major difference in their phonon spectra is expected to arise from the mass difference between Ga and Rh. The zone-centre phonon frequencies of these two compounds are compared in Table II. As one can expect, the highest optical phonon mode lies at nearly the same frequency for both isostructural materials due to the light mass of N atom. The T_{2u} and T_{1u}^2 phonon modes in Cr_3GaN have higher frequencies than their counter-parts in Cr_3RhN due to the mass difference between Ga and Rh atoms. In contrast, the T_{1u}^1 mode of Cr_3RhN lies at a slightly higher frequency than that of Cr_3GaN although the mass of Rh atom is heavier than that of Ga atom. This can be explained by using the separation of the phonon frequency[52] ω^2 into a short-range "normal" part ω_n^2 and a long-range "anomalous" part ω_a^2, $\omega^2 = \omega_n^2 + \omega_a^2$. The first part depends only upon short-range interaction, while the second part is always negative and depends on the electronic screening effects. As the corner atom is changed from Rh to Ga, although ω_n hardens due to decreasing mass, the negative contribution of ω_a^2 becomes higher. This competition leads to a decrease in ω^2 for the T_{1u}^1 mode of Cr_3GaN. As a result, due to stronger electronic screening effects in Cr_3GaN, the T_{1u}^1 mode for this material has a slightly smaller frequency than the corresponding phonon mode of its isostructural compound Cr_3RhN. In order to achieve a clear understanding of the mass effect on the vibrational modes at Γ, we have performed calculations of phonon modes in Cr_3GaN using the force constants for its isostructural compound Cr_3RhN (Ref. 35) but replacing the mass of Rh by that of Ga. We have observed that the frequencies of those T_{1u}^1 and T_{1u}^2 modes that contain considerable contributions from the corner atom (Ga or Rh) are affected by the mass replacement, whereas the frequencies of other species do not change.

Now we discuss the interaction between electrons and phonons. The electron-phonon coupling constant λ is usually extracted from the Eliashberg function as described in our

TABLE II. Calculated vibration modes (in THz) at Γ for Cr_3GaN as compared with its isostructural compound Cr_3RhN.

Material	T_{2u}	T_{1u}^1	T_{1u}^2	T_{1u}^3
Cr_3GaN	2.86	4.02	6.24	19.16
Cr_3RhN (Ref. 35)	1.26	4.76	5.29	19.80
Cr_3GaN[a]	1.26	4.86	5.90	19.80

[a]Vibration modes at Γ of Cr_3GaN obtained using the force constant matrix of Cr_3RhN.

TABLE III. The zone-centre electron-phonon coupling parameters for Cr_3GaN as compared with those of its isostructural compound Cr_3RhN.

Material	T_{2u}	T^1_{1u}	T^2_{1u}	T^3_{1u}
Cr_3GaN	0.72	0.14	0.03	0.02
Cr_3RhN (Ref. 35)	1.98	0.14	0.17	0.02

previous papers (see, e.g., Ref. 46). It may be expected that the phonon modes which interact strongly with high 3d density of states at the Fermi level in Cr_3GaN involve low-frequency vibrations of Cr atoms. These are the acoustic phonon modes as well as the low-frequency T_{2u} mode which directly modifies the Cr-Cr distance. The electron-phonon coupling parameter for different zone-centre phonon modes in Cr_3GaN is compared with those for Cr_3RhN in Table III. Clearly, the largest electron-phonon coupling parameter for both materials has been observed for the low-frequency T_{2u} mode. However, the electron-phonon coupling parameter for the T_{2u} mode of Cr_3GaN is lower than that of Cr_3RhN. The reason for this is that the T_{2u} phonon mode of Cr_3RhN is softer than that of Cr_3GaN. In accordance with the McMillan-Hopfield equation, a softer phonon mode makes a larger contribution to the electron-phonon coupling parameter.

The structural stability of Cr_3GaN under high pressure has been examined in Fig. 6. The structural stability is confirmed by the lack of any imaginary phonon frequencies in the whole Brillouin zone in the pressure range 0–100 GPa. It is clear from this figure that all the phonon modes harden as pressure increases. In particular, the frequency of the T_{2u} mode at the Γ point, dominating the electron-phonon coupling, is greatly increased from 2.86 THz at 0 GPa to 4.99 THz at 100 GPa. The enhanced frequency of this mode contributes to the increase of $\langle\omega^2\rangle$ in the McMillan-Hopfield equation and thus results in the reduction of the electron-phonon coupling parameter. We have observed that the electron-phonon coupling parameter for T_{2u} is considerable decreased from 0.72 at 0 GPa to 0.48 at 100 GPa. The origin of considerable decrease of λ for T_{2u} mode with increasing pressure is mainly attributed to the enhanced frequency of this phonon mode.

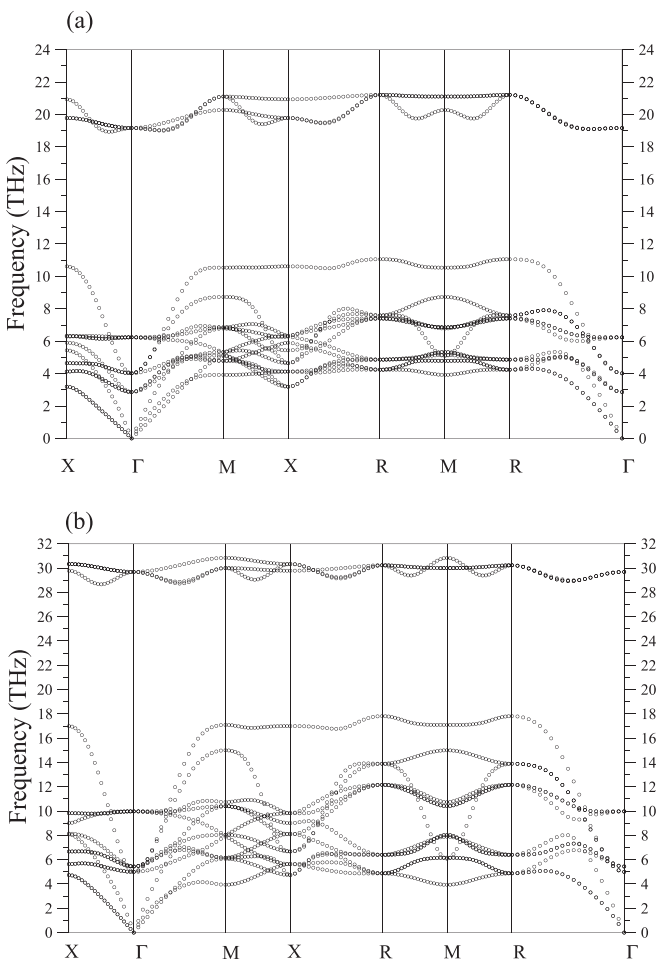

FIG. 6. Calculated phonon spectra of Cr3GaN for (a) normal pressure (0 GPa) and (b) 100 GPa, respectively.

The Eliashberg function $\alpha^2F(\omega)$ of Cr_3GaN is compared with that of Cr_3RhN in Fig. 7(a). From this figure, we can say that the electron-phonon interaction in Cr_3GaN is relatively weaker than the corresponding interaction in its isostructural compound Cr_3RhN. Now, we can compare the average electron-phonon coupling parameter λ for Cr_3GaN with Cr_3RhN. Our computed value of λ for Cr_3GaN is found to be 0.53 which is nearly half of the average electron-phonon coupling value of 1.03 for Cr_3RhN.[34] It should be noted that λ for Cr_3GaN was estimated to be 1.3 in the theoretical work of Wiendlocha *et al.*[34] This result is higher that our result of 0.53. We should, however, note that Wiendlocha *et al.*[34] estimated this parameter without taking phonon properties into account. For Cr_3GaN, we obtain for the logarithmically averaged frequency $\omega_{ln} = 306$ K. Now, in order to obtain the superconductor transition temperature for Cr_3GaN, we need to know the value of μ^*, the effective screened Coulomb repulsion constant. Previous studies[47–49] on transition metals showed that μ^* takes values between 0.1 and 0.16. As Cr is a transition metal, we consider values of μ^* between 0.1 and 0.13 in our study. Inserting the calculated values of λ and ω_{ln} into the Allen-Dynes formula[47–49] with $\mu^* = 0.10$, 0.11, 0.12, and 0.13, we have obtained the superconductor transition temperature $T_C = 4.78$, 4.17, 3.60, and 3.08 K. Our results clearly show that the cubic antiperovskite Cr_3GaN is a superconductor with the value of T_C around 4 K.

All phonon frequencies harden with increasing pressure. This will affect the values of the averaged square of the phonon frequency $\langle\omega^2\rangle$ and the logarithmic-averaged phonon frequency ω_{ln}. These quantities are very important for the electron-phonon coupling parameter because it is well known that the hardening of phonon frequencies make a negative contribution to this parameter. The values of $\langle\omega^2\rangle$ and ω_{ln} increase with increasing pressure. As can be seen from the McMillan-Hopfield expression, the frequency hardening is considered to contribute to the decrease of λ with increasing pressure. Finally, we have illustrated the pressure dependence of the electron-phonon coupling parameter (λ) and the superconductor transition temperature (T_C) in Figs. 7(b) and 7(c). We have observed a monotonically decreased λ from 0.53 at zero pressure 0.43 at 100 GPa. Due to the decrease of λ, T_C also decreases with increasing pressure. T_C has been found to monotonically decrease from 0 to 100 GPa and reaches the value of 2.88 K at 100 GPa for $\mu^* = 0.11$.

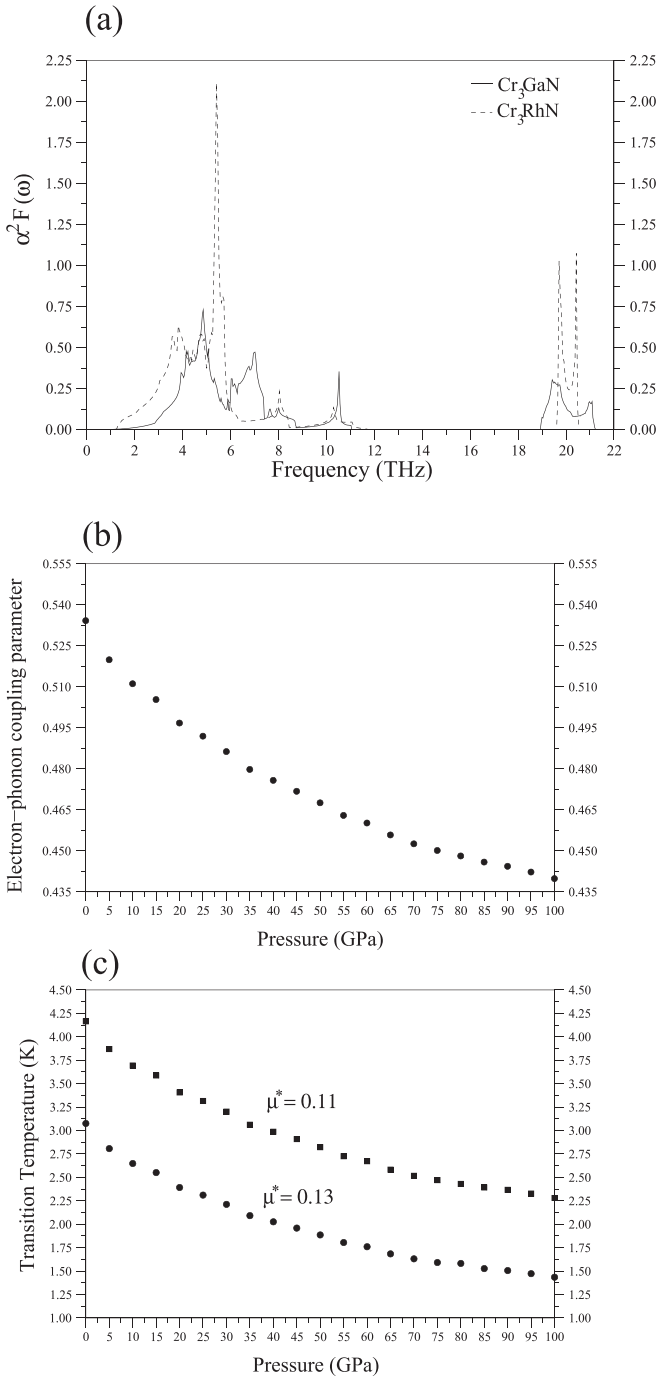

FIG. 7. (a) The calculated electron-phonon spectral function $\alpha^2F(\omega)$ for Cr_3GaN as compared with that of Cr_3RhN. (b) The electron-phonon coupling parameter (λ) as a function of pressure for Cr_3GaN. (c) The superconductor transition temperature (T_C) as a function of pressure for Cr_3GaN. Two choices for μ^* have been made: 0.11 and 0.13.

We now make a comparison as regards superconductivity between Cr_3GaN and its isostructural compound Cr_3RhN by analysing their electronic and phonon structures. We have presented a comparison of the superconducting parameters for these compounds in Table IV. As noted before, three main factors effect T_C: the electronic DOS at the Fermi level $N(E_F)$, the logarithmic average phonon frequency ω_{ln} (or the averaged square of the phonon frequency $\langle\omega^2\rangle$), and the strength of electron-phonon coupling parameter λ. As regards the electronic structure, the calculated $N(E_F)$ value of 5.00 states/eV for Cr_3GaN is smaller than the corresponding value of 6.16 states/eV for Cr_3RhN,[35] making superconductivity comparatively less favourable for Cr_3GaN. The lower energy phonon modes in Cr3GaN are harder than the corresponding phonon modes in Cr_3RhN due to the small mass of Ga atom as compared to the mass of Rh atom. Although harder phonon frequencies lead to larger ω_{ln} and $\langle\omega^2\rangle$ values, they make a negative contribution to the strength of electron-phonon coupling parameter. Consequently, the T_C value of around 4.2 K for Cr_3GaN is considerably lower than the corresponding the value of 17.7 K for Cr_3RhN.[35]

TABLE IV. Comparison of superconducting state parameters for Cr_3GaN and Cr_3RhN. The parameter μ^* is taken to be 0.11.

Perovskite	$N(E_F)$(States/eV)	ω_{ln}(K)	$(\langle\omega^2\rangle)^{1/2}$(K)	λ	T_C(K)
Cr_3GaN	5.00	306	3.88	0.53	4.17
Cr_3RhN (Ref. 35)	6.16	255	339	1.03	17.74

IV. SUMMARY

In this work, we have presented a theoretical analysis of the structural and electronic properties of the cubic antiperovskite Cr_3GaN by using the generalised gradient approximation of the density functional theory and the plane wave pseudopotential method. Our results show metallic d-like bands crossing the Fermi level, indicating that the transition metal Cr may play more active role in the electronic and superconducting properties of this antiperovskite. The effect of pressure is found to redistribute the peaks in the electronic density of states close to the Fermi level: the peaks on either side of the Fermi level are decreased in their height. With pressure increase, $N(E_F)$ decreases monotonically, leading to a reduction of electron-phonon coupling parameter λ. We have shown that the phonon modes related to the vibrations of Cr atoms make a large contribution to the average electron-phonon coupling parameter λ. The computed value of λ is 0.53, and the superconducting critical temperature is estimated to be around 4.2 K.

This compound is predicted to be structurally stable, as there are no imaginary phonon frequencies in the whole Brillouin zone in the pressure range 0.0–100 GPa. All phonon modes shift to higher frequencies when pressure increases. With increasing pressure, the values of logarithmic-averaged phonon frequency ω_{ln} and averaged square of the phonon frequency $\langle\omega^2\rangle$ increase rapidly. On the other hand, the values of $N(E_F)$, λ and T_C decrease with increasing pressure. We strongly believe that reduced $N(E_F)$ and the enhanced frequencies of phonon modes are the main causes for the monotonic decrease of λ, and consequently of T_C with increasing pressure.

A comparison of the superconducting parameters for Cr_3GaN and Cr_3RhN shows that the value of T_C for Cr_3GaN is lower that the corresponding value for Cr_3RhN. This is related to the relatively lower values of the electronic density of states at the Fermi level, the Eliashberg function, as well as the lower average electron-phonon coupling parameter for Cr_3GaN.

ACKNOWLEDGMENTS

The calculations were performed using the Intel Nehalem (i7) cluster (ceres) at the University of Exeter.

[1]T. He, Q. Huang, A. P. Ramirez, Y. Wang, K. A. Regan, N. Rogado, M. A. Hayward, M. K. Haas, J. S. Slusky, K. Inumaru, H. W. Zandbergen, N. P. Ong, and R. J. Cava, Nature (London) **411**, 54 (2001).
[2]Z. Pribulova, J. Kacmarcik, C. Marcenat, P. Szabo, T. Klein, A. Demuer, P. Rodiere, D. J. Jang, H. S. Lee, H. G. Lee, S.-I. Lee, and P. Samuely, Phys. Rev. B **83**, 104511 (2011).
[3]H. Rosner, R. Weht, M. D. Johannes, W. E. Pickett, and E. Tosatti, Phys. Rev. Lett. **88**, 027001 (2001).
[4]J. H. Shim, S. K. Kwon, and B. I. Min, Phys. Rev. B **64**, 180510 (2001).
[5]J.-Y. Lin, P. L. Ho, H. L. Huang, P. H. Lin, Y.-L. Zhang, R.-C. Yu, C.-Q. Jin, and H. D. Yang, Phys. Rev. B **67**, 052501 (2003).
[6]Z. Q. Mao, M. M. Rosario, K. D. Nelson, K. Wu, I. G. Deac, P. Schiffer, Y. Liu, T. He, K. A. Regan, and R. J. Cava, Phys. Rev. B **67**, 094502 (2003).
[7]L. Shan, H. J. Tao, H. Gao, Z. Z. Li, Z. A. Ren, G. C. Che, and H. H. Wen, Phys. Rev. B **68**, 144510 (2003).
[8]J. H. Kim, J. S. Ahn, J. Kim, M. S. Park, S. I. Lee, E. J. Choi, and S. J. Oh, Phys. Rev. B **66**, 172507 (2002).
[9]A. Szajek, J. Phys. Condens. Matter **13**, L595 (2001).
[10]S. B. Dugdale and T. Jarlborg, Phys. Rev. B **64**, 100508 (2001).
[11]I. Hase, Phys. Rev. B **70**, 033105 (2004).
[12]I. R. Shein, V. V. Bannikov, and A. L. Ivanovski, Physica C **468**, 1 (2008).
[13]D. J. Singh and I. I. Mazin, Phys. Rev. B **64**, 140507 (2001).
[14]M. D. Johannes and W. E. Pickett, Phys. Rev. B **70**, 060507(R) (2004).
[15]H. M. Tütüncü and G. P. Srivastava, J. Phys.: Condens. Matter **18**, 11089 (2006).
[16]R. Heid, B. Renker, H. Schober, P. Adelmann, D. Ernst, and K.-P. Bohnen, Phys. Rev. B **69**, 092511 (2004).
[17]H. Hong, M. Upton, A. H. Said, H.-S. Lee, D.-J. Jang, S.-I. Lee, R. Xu, and T.-C. Chiang, Phys. Rev. B **82**, 134535 (2010).
[18]A. Yu. Ignatov, S. Y. Savrasov, and T. A. Tyson, Phys. Rev. B **68**, 220504 (2003).
[19]P. K. Jha, S. D. Gupta, and S. K. Gupta, AIP Adv. **2**, 022120 (2012).
[20]M. Uehara, T. Yamazaki, T. Kori, T. Kashida, Y. Kimishima, and I. Hase, J. Phys. Soc. Jpn. **76**, 034714 (2007).
[21]S. Bağci, S. Duman, H. M. Tütüncü, and G. P. Srivastava, Phys. Rev. B **78**, 174504 (2008).
[22]M. Uehara, A. Uehara, K. Kozawa, and Y. Kimishima, J. Phys. Soc. Jpn. **78**, 33702 (2009).
[23]M. Uehara, A. Uehara, K. Kozawa, T. Yamazaki, and Y. Kimishima, Physica C **470**, S688 (2010).
[24]C. Li, W. G. Chen, F. Wang, S. F. Li, Q. Sun, S. Wang, and Y. Jiaö, J. Appl. Phys. **105**, 123921 (2009).
[25]C. M. I. Okoye, Physica B **405**, 1562 (2010).
[26]Y. Xu, F. Gao, X. Hao, and Z. Li, Comput. Mater. Sci. **50**, 737 (2010).
[27]I. R. Shein, V. V. Bannikov, and A. L. Ivanovskii, Phys. Status Solidi B **247**, 72 (2010).
[28]M. A. Helal and A. K. M. A. Islam, Physica B **406**, 4564 (2011).
[29]M. A. Ali, A. K. M. A. Islam, and M. S. Ali, J. Sci. Res. **4**, 1 (2012).
[30]B. T. Matthias, T. H. Geballe, V. B. Compton, E. Corenzwit, and G. W. Hull, Jr., Phys. Rev. **128**, 588 (1962).
[31]Y. Nishihara, Y. Yamaguchi, T. Kohara, and M. Tokumoto, Phys. Rev. B **31**, 5775 (1985).
[32]Y. Nishihara, Y. Yamaguchi, M. Tokumoto, K. Takeda, and K. Fukamichi, Phys. Rev. B **34**, 3446 (1986).
[33]H. M. Tütüncü, S. Bağci, G. P. Srivastava, and A. Akbulut, J. Phys.: Condens. Matter **24**, 455704 (2012).
[34]B. Wiendlocha, J. Tobola, S. Kaprzyk, and D. Fruchart, J. Alloys Compd. **442**, 289 (2007).
[35]H. M. Tütüncü and G. P. Srivastava, J. Appl. Phys. **112**, 093914 (2012).
[36]S. Baroni, S. de Gironcoli, A. Dal. Corso, and P. Giannozzi, Rev. Mod. Phys. **73**, 515 (2001).
[37]P. Giannozzi *et al.*, J. Phys.: Condens. Matter **21**, 395502 (2009).
[38]J. P. Perdew, K. Burke, and M. Ernzerhof, Phys. Rev. Lett. **77**, 3865 (1996).
[39]D. Vanderbilt, Phys. Rev. B **41**, 7892 (1990).
[40]A. M. Rappe, K. M. Rabe, E. Kaxiras, and J. D. Joannopoulos, Phys. Rev. B **41**, 1227 (1990).
[41]H. J. Monkhorst and J. D. Pack, Phys. Rev. B **13**, 5188 (1976).
[42]A. B. Migdal, Zh. Eksp. Teor. Fiz. **34**, 1438 (1958) [Sov. Phys. JETP **7**, 996 (1958)].
[43]G. M. Eliashberg, Zh. Eksp. Teor. Fiz. **38**, 966 (1960); **39**, 1437 (1960) [Sov. Phys. JETP **11**, 696 (1960)]; **12**, 1000 (1960).
[44]S. Y. Savrasov and D. Y. Savrasov, Phys. Rev. B **54**, 16487 (1996).
[45]R. Bauer, A. Scmid, P. Pavone, and D. Strauch, Phys. Rev. B **57**, 11276 (1998).
[46]H. M. Tütüncü, S. Bağci, and G. P. Srivastava, Phys. Rev. B **82**, 214510 (2010).
[47]W. L. McMillian, Phys. Rev. **167**, 331 (1968).
[48]P. B. Allen, Phys. Rev. B **6**, 2577 (1972).
[49]P. B. Allen and R. C. Dynes, Phys. Rev. B **12**, 905 (1975).
[50]M. Nardin, G. Lorthioir, M. Barberon, R. Madar, E. Fruchart, and R. Fruchart, C.R. Acad. Sci., Ser. IIc: Chim **274**, 2168 (1972).
[51]F. Vines, C. Sousa, P. Liu, J. A. Rodriguez, and F. Illas, J. Chem. Phys. **122**, 174709 (2005).
[52]C. Bungaro, K. M. Rabe, and A. D. Corso, Phys. Rev. B **68**, 134104 (2003).